AIAA SciTech Forum
7-11 January 2019, San Diego, California
AIAA Scitech 2019 Forum

10.2514/6.2019-1527

A Computational Framework for Assessment of Fuel Sloshing Effects on Transonic Wing Flutter Characteristics

S. Srivastava*, M. Damodaran** and B.C. Khoo#

National University of Singapore
Faculty of Engineering, 9 Engineering Drive 1, Singapore 117575

ABSTRACT

The present study focuses on the development and application of a computational framework for assessing the effects of fuel sloshing in internal fuel tanks on the aeroelastic characteristics of aircraft wing configurations. The framework couples an open source compressible flow solver for external aerodynamics, a structural solver for computing the structural motion/deformation and an open source Volume of Fluid (VOF) solver for fuel sloshing in internal wing fuel tanks. As time domain flutter solution of these coupled solvers is computationally expensive, a reduced order model (ROM) is developed for prediction of sloshing loads based on structural inputs. The aim of the ROM is to efficiently describe the dominant static and dynamic characteristics of the underlying system by employing radial basis function neural networks (RBF-NN) to train the dynamic relationship between the structural motions and resulting sloshing loads. A limited CFD-based data is exploited to calibrate the ROM. Hence, a specially designed structural input is required to efficiently capture all the relevant dynamics of the system. A white-noise random signal-based input design method is developed and utilized for the same purpose. The flutter boundary is compared for clean wing section with and without internal fuel tank for different fill levels. The computational framework applied to a wing section with an internal tank has demonstrated promising results motivating feasibility of an extension to a three-dimensional wing with an internal fuel tank.

I. Introduction

Aeroelastic characteristics are an important consideration for modern high-speed aircraft design. Recent research has focused on reductions in emissions, noise and fuel usage. This has a direct consequence of reduction of structural weight and increased wing flexibility, which intensifies the interaction between the aerodynamics and structures and leads to problems such as excessive gust loading, unacceptable flutter margins, and limit cycle oscillations. Fuel sloshing has been shown to have effects on the dynamics of a number of vehicle types, including spacecraft in a variety of studies such as Abrahamson [1] and Vreeberg [2], while Sankar et al. [3] and Kim et al. [4] assessed fluid sloshing effects on tanker-ship hydrodynamics. The numerous effects of sloshing on transonic aircrafts has also been recognized by aircraft design community such as Cazier et al.[5] and Runyan and Morgan[6]. Firouz-Abadi [7] has shown that the wing-store flutter boundary and LCO characteristics of aeroelastic systems gets significantly modified when sloshing effects are considered in the upper subsonic and transonic range. Farhat et al. [8] and Chiu and Farhat [9] used a hydrostatic vibration model to simulate fuel sloshing in a cylindrical store and showed that in general, the critical pressure and flutter speed decrease with increasing fill levels.

Sloshing in fuel tank is excited by aircraft motion, and sloshing affects the global motion in return. Sloshing of fluid in an internal fuel tank subject to external excitation from an aircraft wing generates highly non-linear dynamical systems. To observe the coupling effects of the aircraft and sloshing, the capability of analyzing both problems is

*Graduate Student, Dept. of Mechanical Engineering; shashank.srivastava@u.nus.edu
** Senior Research Scientist, Temasek Laboratories; Associate Fellow AIAA; tslmura@nus.edu.sg
# Professor of Mechanical Engineering and Director Temasek Laboratories; tslhead@nus.edu.sg

essential. The aeroelastic solver and multiphase solver must be coupled in time domain to address sloshing effects on flutter characteristics in time domain analysis. Hence a multi-physics computational model is required to model the effects of sloshing in fuel tanks (internal as well as external) on the aeroelastic behavior of aircraft wings. However, such a coupling is computationally expensive and impractical for time domain solutions. Therefore, the development of reduced order models (ROMs) for such aeroelastic analysis becomes a natural choice for time-marching solutions since calculating the response of a reduced order model is far more efficient and cheaper than solving high-fidelity flow model equations. Lucia et al. [10] and Dowell and Hall [11] provide a comprehensive overview of several reduced-order techniques such as harmonic balance, Volterra theory and Proper orthogonal decomposition (POD), while demonstrating their application to aeroelastic test cases. There are approaches which use linear system identification concepts to obtain a ROM; however, such methods based on state-space approach cannot accurately capture non-linearities of the sloshing model, the large amplitude vibrations and limit cycle oscillations, which require specialized methods for non-linear system identification. Faller and Schreck [12] proposed a recurrent multi-layer-perceptron neural network (MLP-NN) to predict unsteady loads for aeroelastic applications and this study was subsequently followed up by Voitcu and Wong [13] and Mannarino and Mantegazza [14] leading to a systems model aeroelastic behavior of airfoils and wings based on non-recurrent MLP-NN. The dynamic loads of sloshing fluid in a fuel tank not only depends on the current state, but also on the previous states and inputs since the fluid is always in a transition. In order to include dynamic memory effects, temporal derivatives of the excitation signal are to be added to the input vector of the neural network. Neural networks have been shown to offer a powerful tool in modeling nonlinear systems over a compact set rather than a small neighborhood around the dynamically linearized steady state ROM based approach for linear systems. It provides a powerful tool for learning complex input-output mappings and has simulated many studies for identification of dynamic systems with unknown nonlinearities as outlined in a number of studies such as Narendra and Parthsarathy [15] and Elanayar and Shin [16].

The basic idea of the proposed computational procedure in this work is first demonstrated in this study to model the effect of sloshing in internal fuel tanks on aeroelastic behavior of a pitch-plunge wing section model through transonic regime. The model requires coupling of: a compressible flow solver for external aerodynamics, a structural solver for computing the structural motion/deformation and a Volume of Fluid (VOF) [17] solver for modelling fluid sloshing. For the present study, the relation between sloshing loads and structural excitations are considered as black-box and no model structure is assumed a priori. The aim of the developed ROM methods is to efficiently describe the dominant static and dynamic characteristics of the underlying system, i.e. sloshing fluid. Therefore, a limited set of CFD-based data is exploited for calibrating the ROM. Subsequently, the developed ROM can be supplied with new inputs and must respond with accurate load data.

II. Aeroelastic Model

The basic elements of the proposed computational model are first demonstrated for the influence of fuel sloshing in internal tanks on the pitching and plunging motion of a large aspect ratio rectangular planform wing for which a two-degree-of-freedom pitching and plunging model for a wing section will be assumed to be a good approximation. The 2D airfoil flutter model corresponding to NACA641010 airfoil/wing section of Isogai [18] is used first for benchmarking and demonstrating the basic elements of the proposed computational framework. The 2-DOF pitch-plunge model is governed by the following equations:

$$\begin{aligned} m\ddot{h} + S_\alpha \ddot{\alpha} + K_h h &= -L \\ S_\alpha \ddot{h} + I_\alpha \ddot{\alpha} + K_\alpha \alpha &= M_{ea} \end{aligned} \tag{1a}$$

where m is the mass of the wing section (kg/m), S_α is the static imbalance (kg), I_α is the moment of inertia about the elastic axis, K_h is the plunge stiffness (N/m/m), K_α is the pitching spring stiffness (N) and L and M_{ea} are vertical force and pitching moment about the elastic axis respectively. These equations can be re-written in a matrix form as follows:

$$[M]\{\ddot{q}\} + [K]\{q\} = \{F_{aero}\} \tag{1b}$$

where [*M*] and [*K*] are the non-dimensional mass and stiffness matrices, $\{F_{aero}\} = \frac{4}{\pi\mu k_c^2}\begin{Bmatrix} -C_l \\ -2C_m \end{Bmatrix}$ and $\{q\} = \begin{Bmatrix} h/b \\ \alpha \end{Bmatrix}$ are the load and displacement vectors. To motivate the development and application of SROM based on neural networks consider a partially filled fuel tank embedded inside a NACA64A010 wing section subjected to harmonic pitching and plunging motion as shown in Fig. 1(a). The pitch and plunge are measured from the inertial frame fixed to the leading edge at *t=0* in the direction shown in Fig. 1(a). The sign convention of the aerodynamic load coefficients has been followed to be consistent with the open source compressible flow solver SU2 [19] code structure which is used to compute the external compressible transonic aerodynamic flow fields. Such a motion will generate sloshing forces and moments on the tank walls as shown in Fig. 1(b). Figure 1(c) shows a typical temporal variation of the lateral forces on the walls of the tank which is excited by sinusoidal pitching motion with fixed amplitude from CFD simulations.

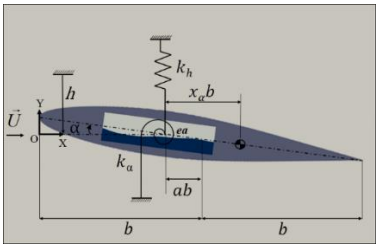

(a)

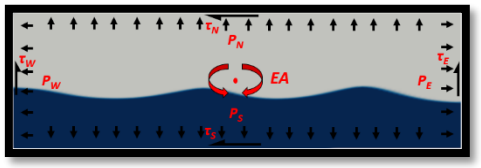

(b)

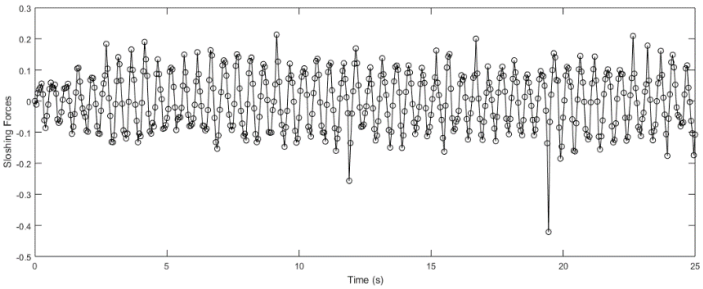

(c)

Figure 1: (a) A NACA64A010 Wing Section with a fuel tank containing sloshing fuel in harmonic pitching and plunging motion built on Isogai's Structural Model (b) A partially filled rectangular fuel tank in sinusoidal pitching motion (c) Typical temporal variation of the sloshing forces on the tank wall obtained from CFD simulations.

The unsteady external aerodynamic flow field is modeled using Euler equation cast into ALE formulation

$$\frac{\partial}{\partial t}\int_{\Omega(t)} \vec{U}\, d\Omega + \int_{\partial\Omega(t)} \vec{F}\vec{n}\, dS = 0 \tag{1c}$$

Where control volume $\Omega(t)$ and its boundary $\partial\Omega(t)$ are time-dependent, $\vec{U}$ denotes the flow variables, $\vec{F}^c(U)$ is convective flux term and $\vec{u}_m$ is the mesh velocity vector. These vectors are defined as

$$\vec{U} = \begin{bmatrix} \rho \\ \rho\vec{V} \\ \rho E \end{bmatrix} \text{ and } \vec{F} = \begin{bmatrix} \rho(\vec{V} - \dot{\vec{u}}_m)\vec{n} \\ \rho\vec{V}(\vec{V} - \dot{\vec{u}}_m)\vec{n} + p\vec{n} \\ \rho E(\vec{V} - \dot{\vec{u}}_m)\vec{n} + p\vec{V}\vec{n} \end{bmatrix} \tag{1d}$$

where $\rho, \vec{V}, E, p$ are the density, the velocity vector, fluid enthalpy and static pressure respectively.

The structural parameters for airfoil model used are are $x_\alpha = 1.8,\ r_\alpha^2 = 3.48,\ \omega_h = 100\ rad/s,\ \omega_\alpha = 100\ rad/s$ and $\mu = 60$, corresponding to Isogai's NACA 641010 wing section. From the flow model one could estimate the time variation of the aerodynamic force and moment coefficients.

III. Modelling of Fuel Sloshing in Fuel Tanks

While a number of models have been used by various researchers as reported in literature, in this work two approaches of different fidelities are used for modeling the sloshing effects of the internal fluid in a rectangular fuel tank to assess its effect on aeroelastic characteristics and flutter prediction. The first approach is based on full order CFD approach which utilizes high fidelity flow computations based on the open source CFD software *OpenFOAM* [20]. The second approach uses a surrogate model to represent the internal fuel sloshing loads on the containing tank. The surrogate model is based on predictive modeling using artificial neural network and is developed as a substitute for high fidelity FOM for quick computations of aeroelastic flutter boundary. Both these models which are briefly outlined below can be integrated with the aeroelastic flutter computational model outlined in Section II.

A. VOF Based CFD Model

The governing equations are the unsteady incompressible Navier-Stokes equations consisting of the conservation of mass or continuity equation:

$$\nabla.\vec{U} = 0 \tag{2a}$$

and the conservation of momentum:

$$\frac{\partial \vec{U}}{\partial t} + (\vec{U}.\nabla)\vec{U} = -\frac{1}{\rho}(\nabla p - \mu(\nabla.\nabla)\vec{U}) + \vec{f}_B + \vec{f}_v \tag{2b}$$

where $\vec{U}$ denotes the velocity of fluid relative to the tank, p the pressure, ρ and μ the density and viscosity, respectively, $\vec{f}_B$ represents the external body forces per unit mass for the fluid due to gravity and $\vec{f}_v$ represents body force per unit mass on the fluid influenced by tank motion. Fuel sloshing in the tank consists of two phases consisting of the fuel and the vapor regions in the tank. The volume of fluid (VOF) method is used for volume tracking in a fixed Eulerian mesh for internal flow in the tank. In this method, a single set of momentum equations is shared by the fluid phases and the volume fraction of each fluid is tracked throughout the domain. A scalar function f is used to characterize the free surface deformation, whose value is set based upon the fluid volume fraction of a cell. The volume fractions are updated by the equation written as

$$\frac{Df}{Dt} = \frac{\partial f}{\partial t} + \vec{U}.\nabla f = 0 \tag{3}$$

After computation of the volume fractions in each cell, the equivalent density ρ_{cell} and viscosity μ_{cell} are estimated as $\rho_{\text{cell}} = \rho_{\text{gas}} + f(\rho_{\text{fuel}} - \rho_{\text{gas}})$ and $\mu_{\text{cell}} = \mu_{\text{gas}} + f(\mu_{\text{fuel}} - \mu_{\text{gas}})$ where ρ_{gas} and μ_{gas} are the density and viscosity of the vapor respectively while ρ_{fuel} and μ_{fuel} are the density and viscosity of the fuel in the tank.

B. Surrogate Model Using Neural Networks

Sloshing fluid is a transient phenomenon therefore previous structural inputs, sloshing loads as well as the current structural input is required for the prediction of the loads for next time step. As fuel sloshing is a transient phenomenon, previous structural state inputs, sloshing loads as well as the current structural state inputs are required for the prediction of the loads for next time step (the future state). One widely used system identification technique is the Autoregressive technique with Exogenous inputs (ARX) as outlined in Billings [21] which assumes that the known relationship between a finite series of former inputs and previous outputs is sufficient to predict system response to subsequent inputs. Such dynamical systems can be written as

$$y(t) = f\begin{bmatrix} u(t), u(t-1), \ldots, u(t-m), \\ y(t-1), \ldots, y(t-n) \end{bmatrix} \tag{4}$$

where *y(k), y(k-1) …* are the predicted outputs i.e. sloshing loads, for the current and previous time steps while *u(k), u(k-1)…* represent the current and previous structural states. This process is shown in Figure 2. Here, it is assumed that *f* is stationary for the system. Such dynamical systems which make use of sequential data and require some '*memory*' of previous states of the systems can be modelled by Recurrent Neural Networks for which delays must be optimized iteratively and the values of *n* and *m* are determined by hit and trial method and theoretically as there are no constraints on limits of their values. For the current study, the inputs and output delay-orders are 5 and 3 respectively.

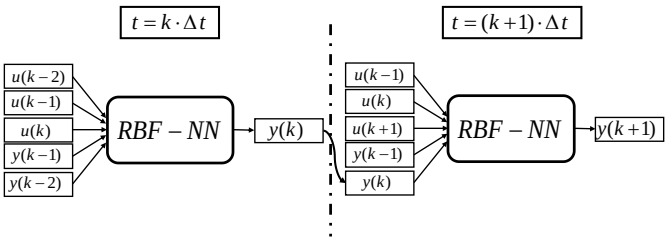

Figure 2: ARX based network with input delay-order of 2 and output delay-order of 1

IV. Computational Framework for Flutter Analysis

The fuel sloshing problem is solved in the time-domain and at each time-step, the sloshing forces and moments acting on the tank wall is obtained by integrating the pressure fields and shear forces along the tank walls. The sloshing loads and consequently, the forces and moments are calculated at the current time step, and the wing section motion is also established for the current time steps. Since the fuel tank is fitted inside the wing section, all the forces and moments acting on the internal walls of the fuel tank can be transferred to the wing section. For the wing section with fuel-tank test model considered in this study, the centroid of the fuel tank is assumed to coincide with the elastic axis of wing section as shown in Fig 1(a). The pressure and shear forces are integrated over the wetted area of the fuel tank walls. The integrated forces/moments on the tank affects the aeroelastic behavior of the wing section. The wing section and subsequently the tank motions, as well as the aerodynamic and sloshing loads are measured relative to the inertial frame represented by X-Y axes in Fig 1(a). The freestream velocity is positive along the X-axis and the lift is measured along the Y axis. The sloshing loads as shown in Fig 1(b), are calculated using the pressure and shear stress data on walls follows:

$$F_{x,sl} = \int_{-h/2}^{h/2} p_E(y) w.dy - \int_{-h/2}^{h/2} p_W(y) w.dy + \int_{-l/2}^{l/2} \tau_S(x) w.dx + \int_{-l/2}^{l/2} \tau_N(x) w.dx \tag{5a}$$

$$F_{y,sl} = \int_{-l/2}^{l/2} p_N(x) w.dx - \int_{-l/2}^{l/2} p_S(x) w.dx + \int_{-h/2}^{h/2} \tau_W(y) w.dy + \int_{-h/2}^{h/2} \tau_E(y) w.dy \tag{5b}$$

and corresponding moment geometric center of the tank is:

$$M_z = \begin{Bmatrix} \int_{-h/2}^{h/2} p_E(y) w(y - y_{EA}) dy + \int_{-l/2}^{l/2} p_N(x) w(x - x_{EA}) dx - \int_{-l/2}^{l/2} p_w(y) w(y - y_{EA}) dy \\ - \int_{-l/2}^{l/2} p_S(x) w(x - x_{EA}) dx + \int_{-h/2}^{h/2} \tau_W(y) w(x - x_{EA}) dy + \int_{-l/2}^{l/2} \tau_N(x) w(y - y_{EA}) dx \\ - \int_{-h/2}^{h/2} \tau_E(y) w(x - x_{EA}) dy - \int_{-l/2}^{l/2} \tau_S(x) w(y - y_{EA}) dx \end{Bmatrix} \tag{5c}$$

The sloshing forces are represented as the vector sum of forces on the wall, and hence there is no need to take special care of inertial forces. The projection of sloshing forces is given by,

$$F_{X,sl} = F_{x,sl}\cos\alpha + F_{y,sl}\sin\alpha \tag{6a}$$

$$F_{Y,sl} = F_{y,sl}\cos\alpha - F_{x,sl}\sin\alpha \tag{6b}$$

$$M_{OZ,sl} = M_{oz,sl} \tag{6c}$$

The sloshing forces acting on the tank wall and the moments can be included on the right-hand side of the aeroelastic eqn 1(b). i.e.

$$[M]\{\ddot{q}\} + [K]\{q\} = \{F_{aero}\} + \{F_{slosh}\} \tag{7a}$$

where

$$\{F_{aero}\} = \frac{4}{\pi\mu k_c^2}\begin{Bmatrix} -C_l \\ -2C_m \end{Bmatrix},\ \{F_{slosh}\} = \begin{Bmatrix} F_{Y,sl} \\ M_{OZ,sl} \end{Bmatrix} \tag{7b}$$

and $F_{slosh} = F_{Y,sl}$ and $M_{slosh} = M_{OZ,sl}$ at each structural time step defined by $\tau_{stuct} = \omega_\alpha t$. After solving the Eq 7(a) and 7(b) at the current time step, the global motion is given to the wing section, and the new position (h and α) is used as the new input to the RBF-NN to predict the new sloshing state (forces and moments). Thus, the coupled equations for the aeroelastic system and sloshing ROM model marches on in time.

As the external aerodynamic forces on the wing section are computed using SU2 and the sloshing forces in the fuel tank inside the wing section are computed using the *InterDyMFOAM* library in *OpenFOAM*. As these are independent solvers these need to be coupled with the structural model for facilitating data transfer via an interface software during the computation. The aeroelastic solver and incompressible internal flow solver interact via transfer of forces and moments and the corresponding structural displacements in time domain at each structural time step. The solvers are coupled via an open-source coupling library for partitioned multi-physics simulations *preCICE* [22] as illustrated in a work flow block diagram shown in the Fig. 3. The existing *preCICE* adapters for *SU2* and *OpenFOAM* are modified to facilitate the coupling. The structural time step is governed by the aeroelastic solver i.e. *SU2* and the pitch-plunge data and sloshing forces and moments are exchanged using the *preCICE Solver Interface* at each structural time step. The existing *su2-adapte*r facilitates writing of the fluid forces and moments to *preCICE* Solver_Interface which can read the structural displacements. The code for the *SU2 preCICE* adapter is modified to read integrated sloshing forces and moments and write structural displacements in form of pitch and plunge motion on to the *preCICE* Solver_Interface. The *openfoam-adapter* is modular in nature and *preCICE* adapter is non-intrusive in nature. This renders higher flexibility for modification of *preCICE* adapter for the current problem. The solver used for fuel sloshing computation in internally attached fuel tank is *interDyMFoam* which is accordingly modified in the adapter. The *preCICE* Solver_Interface writes displacement values to *openfoam-adapter* and reads fluid forces and moments from it.

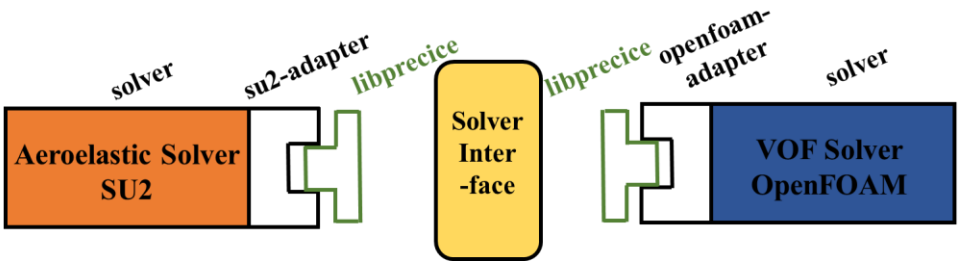

Figure 3: Coupling of aeroeasltic and sloshing solvers using a preCICE interface

V. Surrogate Modeling of Internal Sloshing Using RBF-ANN Approach

The analysis of aeroelastic systems with sloshing tanks requires coupling CFD solvers in time domain. The computational cost of fully coupled model is huge as fuel sloshing must be synchronized with the structure at each computational time step. Hence, it requires development of a surrogate reduced-order model (SROM) to model sloshing effects on the aeroelastic system. The aim of SROM is to efficiently capture and describe the dominant static and dynamic characteristics of the underlying system, i.e. the sloshing loads on the fuel tank. Since the objective of

this study is to model the sloshing forces as an unknown quantity, the approach to handle it should be same as that of a stochastic system. The sloshing forces can become highly nonlinear depending upon the motion on containing structure and hence localized pressure prediction may be difficult, but it is the integrated force/moment on the tank that affects the motion of the container. Therefore, a limited CFD -based data is exploited to develop and calibrate the SROM which predicts integrated forces and moment on the fuel tank for subsequent structural motions fed in as inputs. Neural-network-based surrogate modeling approach is apt for the given problem. Although this approach requires large quantity of training data, the computational cost of a wisely chosen training data set is still very small as compared to full order model.

The generation of the training data by structural excitation for the development of SROM is outlined briefly. Before an input signal is selected, it is important to identify the operating range of the system. Special care must be taken not to excite the dynamics that must not be incorporated in the model. For identification of linear systems, it is customary to apply signals consisting of sinusoids of different amplitudes or impulse inputs. However, for nonlinear model structures it is important that all amplitudes and frequencies are represented. For the current study, the amplitude-modulated pseudo-random binary signal (APRBS), also referred to as *N-samples-constant*, is chosen for forced structural excitation to develop an input-output relation for surrogate modeling. This signal can be generated from frequently used pseudo-random binary signal (PRBS) by assigning random amplitudes to each plateau level. If *e(t)* is a white noise signal with variance σ_e^2, the signal defined by

$$u(t) = e\left(\text{int}\left[\frac{t-1}{N} \right] + 1 \right) \qquad t = 1, 2, \ldots \tag{8a}$$

will jump to a new level at each N^{th} sampling instant (int denotes the integer part) and its covariance function is defined as:

$$R_u(\tau) = \frac{N-\tau}{N}\sigma_e^2 \tag{8b}$$

This signal is further modified by introducing a level change parameter with probability, α = 0.5, for deciding when to change level as follows:

$$u(t) = \begin{cases} u(t-1) \text{ with probability } \alpha \\ e(t) \quad \text{with probability } 1\text{-}\alpha \end{cases} \tag{8c}$$

This modification may be considered as some type of low pass filtering. Normalized white noise signal shown in Fig 4(a) is utilized for constructing ARPBS signal which contains frequencies relevant to the system as shown in Fig. 4(b). The APRBS signal is further modulated with level change modification is shown in Fig. 4(c). The amplitude response to frequency as shown in Fig. 4(d) shows that the level change parameter can be tuned to excite the frequencies of interest.

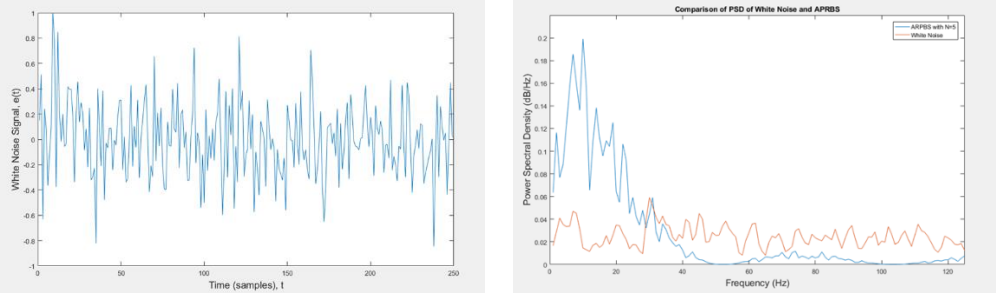

(a) (b)

Fig 4(a) White noise signal used to generate APRBS and cut off higher frequencies (b) Power spectral density comparison of APRBS and white noise signals (c) APRBS with level change modulation (d) Amplitude response to excitation frequencies comparison between APRBS with and without level change parameters (Continued)

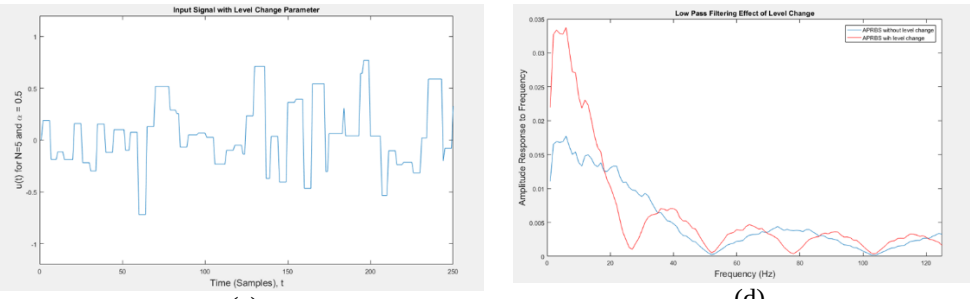

(c) (d)

Fig 4(a) White noise signal used to generate APRBS and cut off higher frequencies (b) Power spectral density comparison of APRBS and white noise signals (c) APRBS with level change modulation (d) Amplitude response to excitation frequencies comparison between APRBS with and without level change parameters

The main advantage of utilizing the APRBS is the large spectrum of frequencies and amplitudes. This property is of paramount importance for the nonlinear system identification task. Furthermore, only a short excitation time-series is needed, limiting the computational cost. Markov chain-based approach is used for training the dynamic system behavior using finite setoff input-output data samples. Radial basis function based neural network (RBF-NN) is used for the current study. The mathematical formulation for a RBF-NN with an output vector consisting of N_y elements $(1 \le i \le N_y)$ can be written as

$$\tilde{y}_i = \sum_{j=0}^{M} w_{ij} . \varphi_j \left(\| u - c_j \| \right) \quad \text{with } \varphi_0 = 1 \tag{9}$$

where $\tilde{y}_i$ is the *i-th* element of the output vector, W is a matrix containing linear weights w_{ij}, u is the input vector and c_j the center vector affiliated to the neuron j. Figure 5 shows the schematic representation of Eqn. (9).

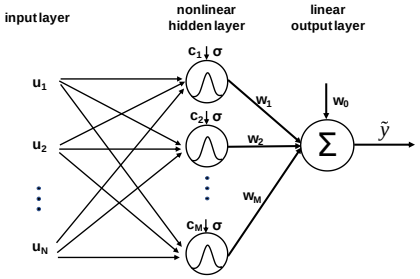

Figure 5: Schematic representation of a RBF-NN with one output *y* and a constant spread σ

For the *M* basis functions φ_j in the hidden layer, the typical approach of using the Gaussian RBF in combination with the Euclidean distance norm is inserted as follows:

$$\varphi_j(\| u - c_j \|) = \exp\left(- \frac{\sum_{k=1}^{N} (u_k - c_{jk})^2}{2\sigma_j^2} \right) \tag{10}$$

VI. Results and Discussions

In order to demonstrate the feasibility of the proposed computational framework a NACA64A010 wing section with an embedded rectangular fuel tank is considered. External flow is considered to be inviscid (done only for the purpose of saving computational costs for this study) while the sloshing in the tank is considered to be viscous.

A. Grid Dependence Studies for the Inviscid Aeroelastic Solver within SU2

A NACA64A010 wing section is immersed in an external inviscid flow governed by Euler equations. The flow is transonic with Mach number 0.70 and the wing section is fixed at 3° angle of attack. The freestream temperature and pressure are 288.15 K and 101325.0 Pa respectively. The variation of coefficient of lift C_L is for 4 grids with the inverse of the mesh size N corresponding to Grid 1, Grid 2, Grid 3 and Grid 4 consisting of about 2300, 4000, 8100 and 16000 elements respectively as shown in Fig. 6(a). Fig 6(b) shows mesh structure in the vicinity of the wing section for Grid 3.

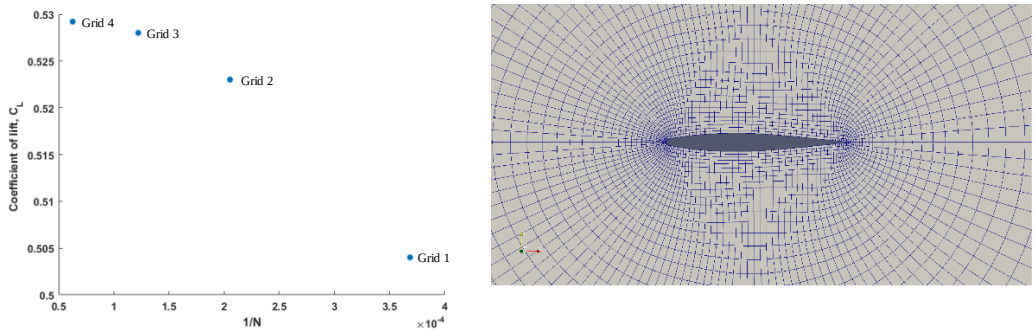

Figure 6: (a) C_L vs. 1/N Variation(b) Grid 3 mesh in the vicinity of the wing section

The grid convergence index is estimated as outlined in Roache [23]. The coefficient of lift is tracked to evaluate the order of convergence $p = \left(\ln\left[\left(f_3 - f_2\right)\left(f_2 - f_1\right)^{-1}\right]\right)\left(\ln(r)\right)^{-1}$ with a refinement ratio, r =1.5 for the grids used in current study, i.e. grids 2, 3 and 4 and where f_1, f_2 and f_3 are the values of C_L computed on the finest, medium and coarsest mesh respectively. For the Grid 3 with nearly 8100 elements, the grid convergence index $GCI = F_S\left|\left(f_2 f_1 - 1\right)\right| r^{-p} - 1$ works out to 0.0017 for a factor of safety F_S of 1.25. This lies in the acceptable range of uncertainty and hence medium grid is used to compute the aeroelastic behavior.

B. Validation of Compressible Flow Solver SU2 for the Inviscid Flutter Analysis of NACA64A010

The compressible flow solver SU2 is validated against numerical results presented by Alonso [24] for the case of the flutter of the NACA64A010 wing section which is forced sinusoidally in pitch for 2 complete cycles at a frequency close to the natural pitching frequency of the structure and then released for free motion. The three typical aeroelastic responses i.e., damping response, neutrally stable response and diverging response at different Mach number values and different values of speed index and $\Delta\alpha = 1^{\circ}, \omega_f = 100$ rad/sec have been replicated in the current study as shown in Fig. 7.

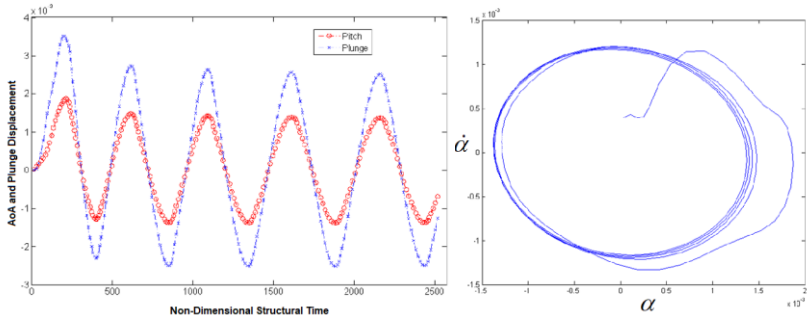

(a)

Figure 7: (a) Neutral response M_∞ = 0.825,V_f = 0.612 (b) Damped response M_∞ = 0.85,V_f = 0.439 (c) Diverging (flutter) response M_∞ = 0.875,V_f = 1.420 (Continued)

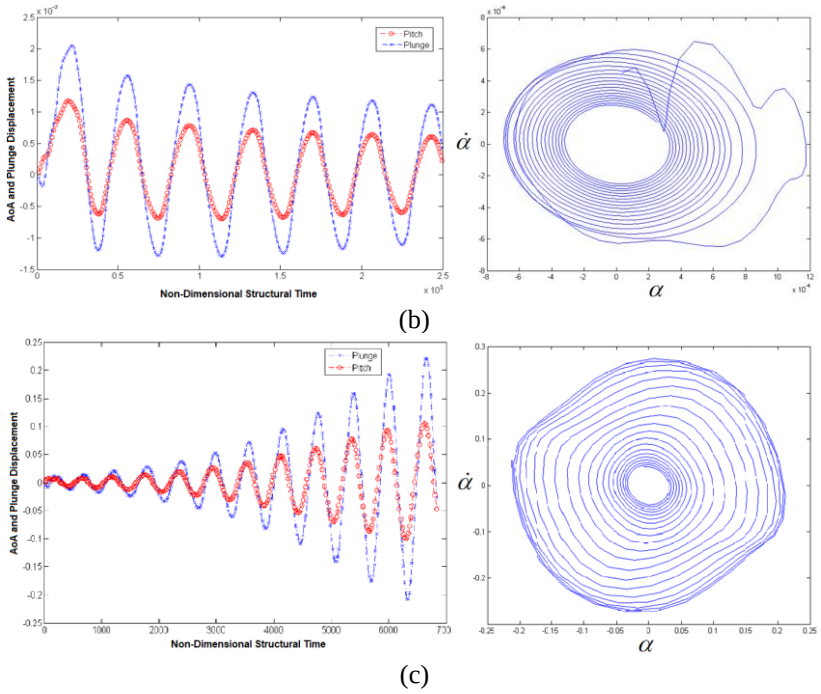

Figure 7: (a) Neutral response $M_\infty = 0.825, V_f = 0.612$ (b) Damped response $M_\infty = 0.85, V_f = 0.439$ (c) Diverging (flutter) response $M_\infty = 0.875, V_f = 1.420$

Figure 8 compares the computed flutter boundary is at four Mach numbers using time-domain solver SU2. At each Mach number, the flutter speed index is fixed and the wing section is forcibly pitched for cycles with 1° amplitude at its natural frequency, i.e. $\omega_\alpha = 100\, rad/s$. The generates an initial flowfield for aeroelastic computations and the wing section is set free to move for five cycles. The resulting motion is checked for damped, neutral or diverging response. The pitch and plunge motion and the phase plot is used to identify the onset of flutter. In Fig. 8 for $M_\infty = 0.80$, the flutter speed index is varied starting from $V_f = 0.78$, until $V_f = 0.86$, where the onset of flutter is observed. The pitch and plunge plots and phase plots are shown for damping aeroelastic response at $V_f = 0.78$ and flutter response at $V_f = 0.86$.

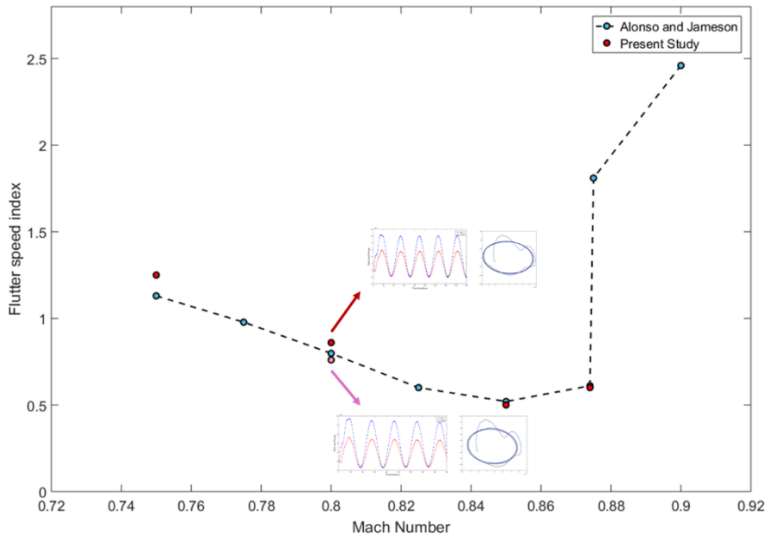

Figure 8: Flutter boundary computation and comparison with Alonso and Jameson [24]

C. Unsteady Sloshing Force Predictions Using Surrogate Model and Validation Using CFD

The constructed neural network (RBF-NN) outlined in Section V is trained using pitching data of rigid fuel tank using N-sample constant structural excitation inputs as shown in Fig. 9 which are designed by exciting natural pitching frequency of the wing section i.e. $\left(\omega_\alpha = 100\, rad/s\right)$ and average pitching amplitude corresponding to first 5 cycles from onset of flutter. Other forms of signals can also be used for this purpose. The sloshing forces on the tank wall obtained from CFD data as output corresponding to structural excitation input are divided into training data and testing data. About 90% of these data are utilized in training of the neural network, i.e. calculation of weights and centers. The remaining 10% data are used for model validation. The RBF-NN prediction is compared against CFD data and the prediction error is found to be less than 8%.

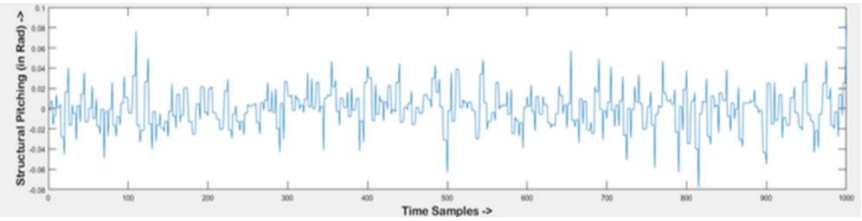

(a)

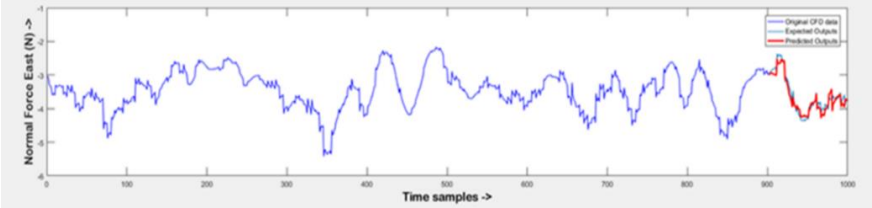

(b)

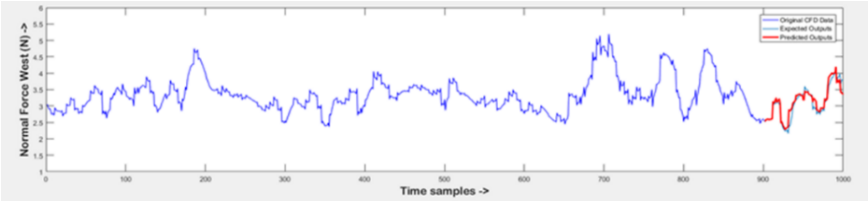

(c)

Figure 9: (a) The structural input provided as pitching angle to fuel tank, (b) comparison of forces on east wall using CFD output and surrogate model prediction, and (c) comparison of forces on west wall using CFD output and surrogate model prediction

Structural motion to the tank is given in the form of a pitching excitation for validating the predictions from proposed SROM approach. The APRBS signal shown in Fig. 9(a) is used as a pitching input to the fuel tank and the corresponding response forces obtained from CFD on the lateral walls (east and west) of the tank are shown in Fig. 9(b) and Fig. 9(c) respectively (in blue line). The forces predicted from the SROM approach are shown in red lines on the same plots and it can be seen that the force predictions from the SROM are in good agreement with those from CFD predictions.

The loads due to sloshing of fluid inside a tank in motion are calculated by integrating the pressure values at the boundary points of the fuel tank at each structural time step. It is worthwhile to study the nature of forces acting due to pitching motion of the tank attached to the wing section at its natural frequency, i.e. 100 rad/sec. The amplitude of

pitching angle is set as 1° and the resulting forces in the lateral direction is plotted as a time series. The forces due to sloshing are estimated at every *t=0.02 s* physical time for a total time of *T = 4 seconds*.

Ibrahim [25] has used a potential flow formulation to estimate the forces due to sloshing as

$$\frac{F}{-i\Omega^2 m_{liq} h\alpha_0} = \frac{1}{12}\left(\frac{a}{h}\right)^2 + 8\left(\frac{a}{h}\right)\sum_{n=1}^{\infty}\frac{\tanh\left[(2n-1)\pi h/a\right]}{(2n-1)^3\pi^3}\left(\frac{1}{2} - \frac{\tanh\left[(2n-1)\pi h/a\right]}{(2n-1)\pi h/2a} + \frac{g}{h\omega_n^2}\right)\left(\frac{\Omega^2}{\omega_n^2 - \Omega^2}\right) \quad (11)$$

where m_{liq} is the mass of liquid, *a*, is the fluid level, *h* is the tank depth, *n* correspond to the sloshing mode, ω_n is the modal natural frequency and Ω is the forcing frequency. A comparison of lateral forces from sloshing computed using CFD and the potential flow formulation for pitching motion is shown in Fig. 10 which shows that the sloshing forces at high frequencies are highly nonlinear and that the linear potential theory cannot correctly predict these loads. Although in the past researchers have used such low order models for estimating sloshing induced forces, in this work which use nonlinear models such as CFD or SROM, it is necessary to use nonlinear models for the correct computation of sloshing loads.

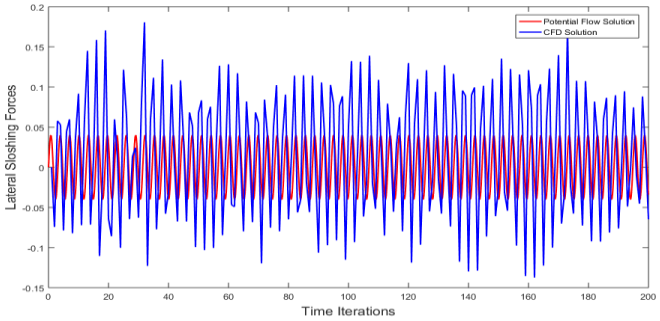

Figure 10: Lateral forces acting on the tank walls as a result of fuel sloshing due to pitching motion of the fuel tank at *f = 15.91 Hz* using CFD and potential flow solution

D. Wing Section Flutter Analysis Using the Computational Framework

The full CFD simulation of multiphase sloshing flow coupled with aeroelastic solver of *SU2* using modified *preCICE* adapters for both solvers and flutter boundary computations are done for different mach numbers by varying the flutter speed index for each Mach number and analyzing the aeroelastic response. The fill level of tank is fixed to 50% and the flow field is initiated with developed flow for pitching excitation at natural frequency and forced excitation amplitude of the containing wing section. The computed external aerodynamic flowfield is initialized by forced pitching the wing section immersed at the required flow conditions as specified earlier. This provides an initial disturbance in external flowfields, which is required for initiating the aeroelastic computation of a symmetric wing section. The free motion of the wing section is captured for first five cycles and the aeroelastic motion is determined thereafter. The computed Mach contours external flowfield at selected instants of time during the unsteady motion starting from the initial state are shown in Fig. 11. The steady state flowfield is computed first as shown in Fig.11(a) and it is used to initialize forced pitching motion. Similarly, the flowfield obtained at the end of forced motion shown in Fig. 11(b) is utilized to describe initial flow conditions for free motion of the wing section. This process not only provides an initial perturbation to the wing section, but also speeds up the computations. Finally, Fig. 11(c) and 11(d) show the flowfield around the wing section during its free motion, which in this case is diverging pitching and plunging. Similarly, the fuel tank is forcefully pitched for 2 cycles and flowfield is initialized for free motion of tank attached with wing section. The initial state of fluid in tank is shown in Fig. 12(a), which has 50% fill level. The perturbed fuel-vapor interface location after 2 forced pitching cycles is shown in Fig.12(b). This is followed by free motion of the fuel tank (rigidly attached to and moving with the wing section) and fuel volume fraction is shown for 2 instances in the 5th cycle of motion in Fig. 12(c)-(d).

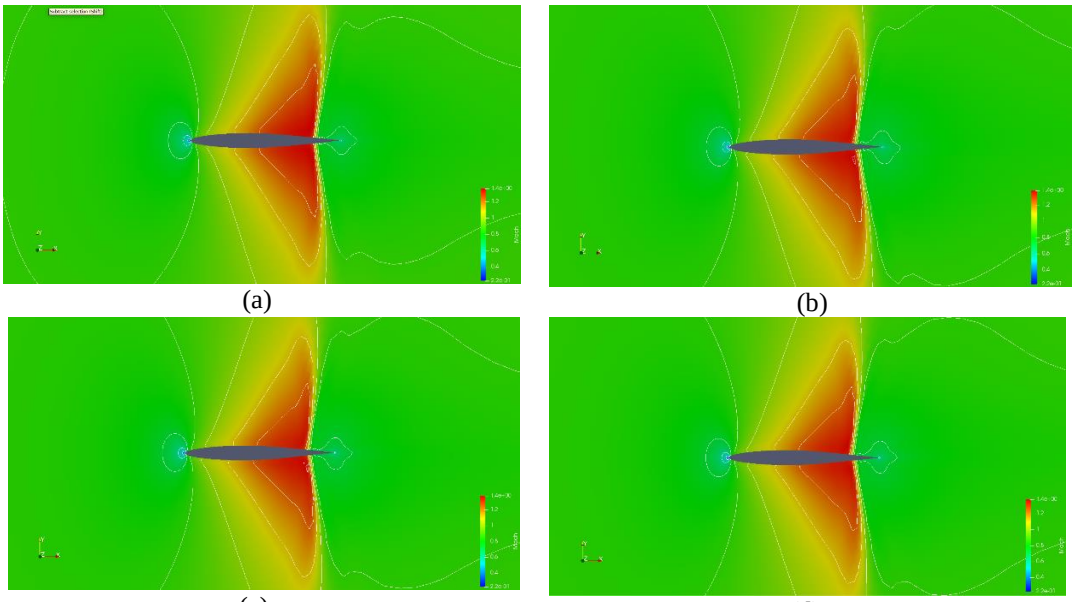

Figure 11: (a) Computed Mach contours for steady state flow past NACA64A010 at Ma = 0.80 and V_f = 0.70 , (b) Unsteady flowfield at the end of 2 forced pitching cycles, (c) Wing Section in $\pi/4$ position in the 5th free cycle going into flutter, and (d) Wing Section at the end of 5th free cycle

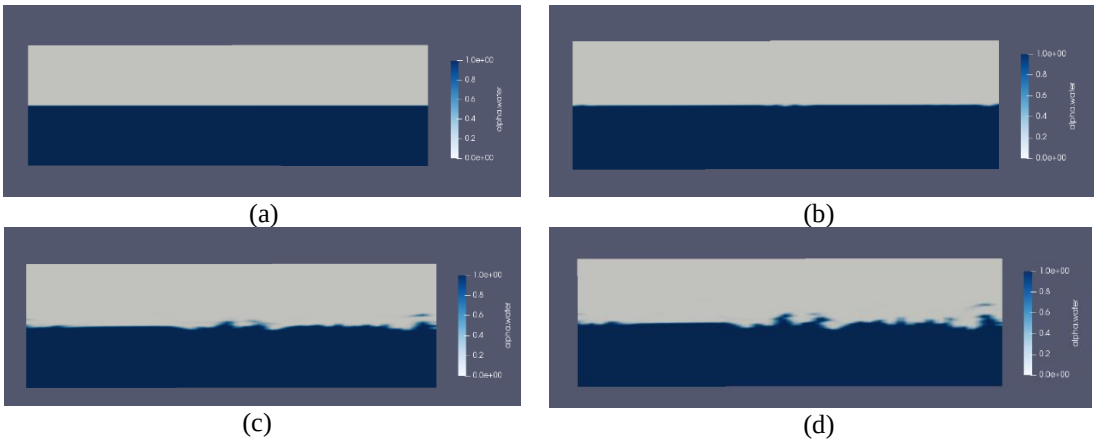

Figure 12: (a) Volume fraction of fuel in rectangular container (50% fill level), (b) Free surface at the end of 2 forced pitching cycles (c) Tank at $\pi/4$ position in the 5th free cycle, and (d) Tank at the end of 5th free cycle

The surrogate model is trained by providing structural motion to the fuel tank in form of a combined pitching and plunging. APRBS signal, as described in section V. This signal is used as the input motion to the embedded tank inside the wing section and corresponding sloshing loads in terms of lateral forces, vertical forces and moment about pitching axis are the target outputs. As these outputs are very similar to those shown in Fig. 9 the plots corresponding to this combined pitch plunge motion of the fuel tank are not shown here. The predicted sloshing forces and moments from the SROM for the combined pitching and plunging motion of the fuel tank are used to compute the aeroelastic response of the wing section due to external aerodynamic loads and sloshing loads quickly. Flutter boundary points are computed by fixing the Mach number and incrementally increasing the flutter speed index. The aeroelastic response is analyzed in time domain and first sign of divergence is marked as the onset of flutter, as shown in Fig. 13 which compares the flutter boundary predicted using the full CFD model (FOM) and the SROM model considering the

effects of fuel sloshing in the embedded fuel tanks with that without sloshing effects and also with the published data from Alonso and Jameson [24].

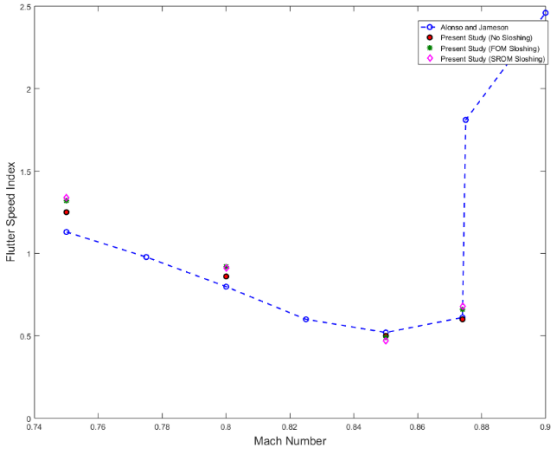

Figure 13: Flutter boundary of NACA64A010 with and without fuel sloshing effects modeled by CFD and SROM

The primary focus of this work is to develop a framework to study the effects of sloshing fuel in an internal tank on the flutter characteristics of aeroelastic systems. Keeping in mind the nonlinear nature of external aerodynamics as well as sloshing of fluid, two approaches of different fidelities are adopted to simulate the effects of internal sloshing in time domain. The aerodynamics, however, has been computed using CFD in time domain for all cases. The coupling of *SU2* and *OpenFOAM* solvers are accomplished using the modified *preCICE* libraries. However, this method is computationally expensive, and it is not very practical for parametric variations of fuel levels, wing section geometry and flow conditions. Hence, a novel surrogate modeling approach is developed using radial basis function based neural networks (RBF-NN) to integrate VOF based sloshing loads with the aeroelastic system. The surrogate model successfully predicts the sloshing loads acting on the tank walls when subjected to white-noise based N-sample constant inputs. The flutter boundary is computed for NACA64A010 with and without the sloshing forces. The flutter boundary is modified by the sloshing effects of fluid inside fuel tank. These results correspond to particular fill level (50%) in the tank, the density and viscosity of the fluid is also fixed as well as the tank size and geometry. Each of the aforementioned factors will affect the flutter boundary and at this stage their sensitivities to flutter computations is not known. The present framework can be utilized to study each factor individually. The SROM developed in this work provides a basis motivating for fast prediction of flutter boundary and the onset of flutter.

VII. Concluding Remarks

The sloshing loads are represented as time series, with specifically designed structural motion as inputs and normal and shear forces as outputs, are modeled by radial basis function neural network based (RBF-NN) ROM. The structural input is designed to excite dynamics of fuel tank around the natural frequency of NACA64A010, i.e. 15.91 Hz so that the dominant dynamics of the sloshing fluids can be captured in the relevant frequency range. The amplitude of motion of structural inputs are modulated according to the aeroelastic response of the wing section. The input-output model is trained and validated by the same CFD based load data. Since the structural input is highly chaotic in nature, the model can predict aeroelastic response with acceptable accuracy. Although N-sample constant based structural inputs are good for nonlinear system identification and validation of prediction of surrogate model, a more realistic input structural excitation would be harmonic motions. The structural input can be further optimized to reduce training sample computational size. The current work aims to demonstrate the effect of fuel sloshing on flutter boundary of an aeroelastic system using potential flow model and a CFD based surrogate modeling approach. A novel model of data prediction is developed which reduces the cost of time-domain coupled computation tremendously. The current computational framework will be enhanced further by considering viscous external flow and extended to a full three-dimensional supercritical wing containing an internal fuel tank. Furthermore, the surrogate reduced order model results will be compared against full order CFD model coupled in time domain to estimate the accuracy of predicted results and to compare the computational savings.

References

[1] Abramson, H.N., "The Dynamic Behavior of Liquids in Moving Containers with Applications to Space Vehicle Technology," Report SP-106, NASA, 1966

[2] Vreeburg, J., "Measured states of sloshsat FLEVO", *Proceedings of 56th International Astronautical Congress*, 2005, Fukuoka, Japan

[3]Sankar, S., Ranganathan, R. and Rakheja, S., "Impact of Dynamic Fluid Slosh loads on the directional response of tank vehicles," *Vehicle System Dynamics* 21(6),385–404, 1996

[4] Kim, Y., Nam, B.W., Kim, D.W. and Kim, Y.S., "Study on coupling effects of ship motion and sloshing," *Ocean Engineering*, Vol. 34, pp. 2176–2187, 2007.

[5] Cazier, F. W. Jr., Doggett, R. V., Jr., and Ricketts, R. H., "Structural Dynamic and Aeroelastic Considerations for Hypersonic Vehicles," *NASA TM-104110*, 1991

[6] Runyan, H. L. and Morgan, H. G., "Flutter at Very High Speeds," *NASA TN-D-942*, 1961

[7] Firouz-Abadi, R.D., Zarifian, P. and Haddadpour, H., " Effect of Fuel Sloshing in the External Tank on the Flutter of Subsonic Wings," *Journal of Aerospace Engineering*, Vol. 27, No. 5, 2014.

[8] Farhat, C., Chiu, E.K., Amsallem, D., Schotte, J.S. and Ohayon, R., "Modeling of Fuel Sloshing and its Physical Effects on Flutter," *AIAA Journal*, Vol. 51, No. 9, pp - 2252-2265, 2013 DOI: 10.2514/1.J052299

[9] Chiu, E.K. and Farhat, C., "Effects of Fuel Slosh on Flutter Prediction*," AIAA 2009-2682, 50th AIAA/ASCE/AHS/ASC Structures, Structural Dynamics, and Materials Conference*, 4-7 May 2009, Palm Springs, CA, USA

[10] Lucia, D.J., Beran, P.S. and Silva, W.A., "Reduced-Order Modeling: New Approaches for Computational Physics*," Progress in Aerospace Sciences*, Vol. 40, pp. 51-117, 2004.

[11] Dowell, E.H. and Hall, K.C., "Modeling of Fluid-Structure Interaction," *Annual Review of Fluid Mechanics*, Vol. 33, pp. 445-490, 2001.

[12] Faller, W.E. and Schreck, S. J., "Unsteady Fluid Mechanics Applications of Neural Networks," AIAA-95-0529, *33rd Aerospace Sciences Meeting and Exhibit*, 9-12 January 1995, Reno, NV

[13] Voitcu, O. and Wong, Y.S., "A Neural Network Approach for Nonlinear Aeroelastic Analysis," *43rd AIAA/ASME/ASCE/AHS,ASC Structures, Structural Dynamics, and Materials Conference*, 22-25 April 2002, Denver, Colorado, USA, 2002

[14] Mannarino, A. and Mantegazza, P., "Nonlinear Aeroelastic Reduced Order Modeling by Recurrent Neural Networks," *Journal of Fluids and Structures*, Vol. 48, pp. 103-121, 2014.

[15] Narendra, K.S. and Parthasarathy, K., "Identification and Control of Dynamical Systems Using Neural Networks," *IEEE Trans. Neural Networks*. 1(1990) 4–26

[16] Elanayar, S. and Shin, Y., "Radial Basis Function Neural Network for Approximation and Estimation of Nonlinear Stochastic Dynamic Systems," *IEEE Trans. Neural Networks*.(1994)594–603

[17] Hirt, C.W. and Nicholas, B.D., "Volume of Fluid Method for the Dynamics of Free Boundaries," *Journal of Computational Physics*, Vol 39, pp. 201-225, 1981

[18] Isogai, K., "On the Transonic-dip Mechanism of Flutter of a Sweptback Wing", *AIAA Journal*, Vol. 17, No. 7, 1979, pp. 793-795.

[19] Economon, T. D., Palacios, F., Copeland, S. R., Lukaczyk, T. W. and Alonso, J. J., "SU2: An Open-Source Suite for Multiphysics Simulation and Design," *AIAA Journal*, Vol. 54, No. 3, 2016, pp. 828-846. https://su2code.github.io/

[20] The OpenFOAM Foundation, "OpenFoam V.5 User Guide", (2011-2018) https://cfd.direct/openfoam/user-guide/

[21] Billings, S.A., "Nonlinear System Identification: NARMAX Methods in the Time, Frequency, and Spatio-Temporal Domains, Wiley, ISBN 978-1-1199-4359-4, 2013

[22] Bungartz, H.J., Gatzhammer, B., Lindner, F., Mehl, M., Scheufele, K., Shukaev, A., and Uekermann, B., *In Computers and Fluids*, Volume 141, p. 250—258. Elsevier, 2016

[23] Roache, P.J., "Verification and Validation in Computational Science and Engineering," Hermosa Publishers, Albuquerque, New Mexico, 1998

[24] Alonso, J.J. and Jameson, A., " Fully-Implicit Time Marching Aeroelastic Solutions," State Paper Number AIAA-94-0056, *32nd Aerospace Sciences Meeting & Exhibit*, January 10-13, 1994, Reno, NV, USA.

[25] Ibrahim, R.A., "Liquid Sloshing Dynamics: Theory and Application," Cambridge Press, 2005